Loess-derived polygenetic soils of North-Western Italy: A deep characterization of particle size, shape and color to draw insights about the past

Sara Negri[a], Elisa Raimondo[a], Michele E. D'Amico[a], Silvia Stanchi[a,*], Angelo Basile[b], Eleonora Bonifacio[a]

[a] University of Torino, Department of Agricultural, Forest and Food Sciences, Largo Braccini 2, 10095 Grugliasco, Italy
[b] Institute for Mediterranean Agricultural and Forest Systems (ISAFOM), National Research Council (CNR), 80056 Ercolano, Italy

ARTICLE INFO

Keywords:
Loess
Image analysis
Loess cycles
Particle-size distribution

ABSTRACT

The multiplicity of units present in a single loess bed greatly complicates the reconstruction of the history of polycyclic loess-derived soils. The present study implemented a combination of techniques to characterize different depositional events in a pedogenized loess formation of North-Western Italy. Field morphological observations, laboratory Particle Size Distribution (PSD) analyses, and single-grain image processing techniques were applied.

Five different loess depositions, or cycles, were distinguished in the field. Laser PSD curves highlighted the fine nature of the studied loess, which stood out even in comparison to similar Italian loess-derived soils. All PSD functions showed a tri/bimodal distribution with a dominant peak at 8–14 μm, wider in younger depositions. The second most relevant peak, at 0.5–4 μm, displayed a greater intensity in older cycles where it also fell in correspondence of slightly bigger particles. The fine-grained nature of the loess was read as a sign of its alluvial origin, therefore the Po plain has been addressed as the source of the material. This hypothesis was supported by evidence of a dominant SE-to-NW paleo-wind direction, proved by the spatial trends of the coarse and fine silt fractions. The typical aeolian size-dependant depositional trait of one of the cycles (IV) was however opposite to that of the other four loess depositions. Therefore, the source of this material was attributed to a site North of the study area where, right behind the Lanzo ultramafic massif, an ice lobe stretched during the Last Glacial Maximum (LGM). Image analysis supported this hypothesis: as the loess grains of cycle IV were significantly darker colored than the others, this would agree with the provenance from an ultramafic source. In conclusion, the variety of applied techniques allowed us to combine different pieces of information in order to assess the physical and morphological properties of the studied loess-derived soils, trying to determine the most probable sources of the material and the weathering pathways.

1. Introduction

Loess is a wind-transported silty sediment mainly originated by the grinding action of glaciers on rocks (Smalley and Marković, 2014). Through this process, rock outcrops are subjected to fragmentation, and the resulting material experiences a long-haul transport. Silt-sized particles are washed away by proglacial flows, deposited close to moraines, exposed to freeze-thaw cycles, and, finally, re-transported by wind (Delage et al., 2005). After deposition, loess is reworked by soil formation, solifluction, and cryoturbation (Muhs and Bettis, 2003).

Loess sheets, mainly remnants of the glacial phases of the Pleistocene, currently cover up to 10% of Earth's surface (Haase et al.,

2007). In Europe, the largest loess belt stretches from Paris to Krakow (Smalley and Leach, 1978), with minor loess covers located in the Carpathians and in the Dacian and Pannonian basins. Loess deposits can be extremely variable in thickness, considering that some exceptional Bulgarian sediments were found to be more than 100 m thick (Haase et al., 2007). The presence of discontinuous loess covers in Northern and Central Italy, mainly alongside the Po Plain and the Pre-Alps, has been widely acknowledged (e.g. Costantini et al., 1996; Haase et al., 2007; Zerboni et al., 2015).

In general, a loess bed is characterized by the presence of multiple stratigraphic units that originated in different periods. A wide temporal range can elapse between older and younger portions. In Southern Italy,
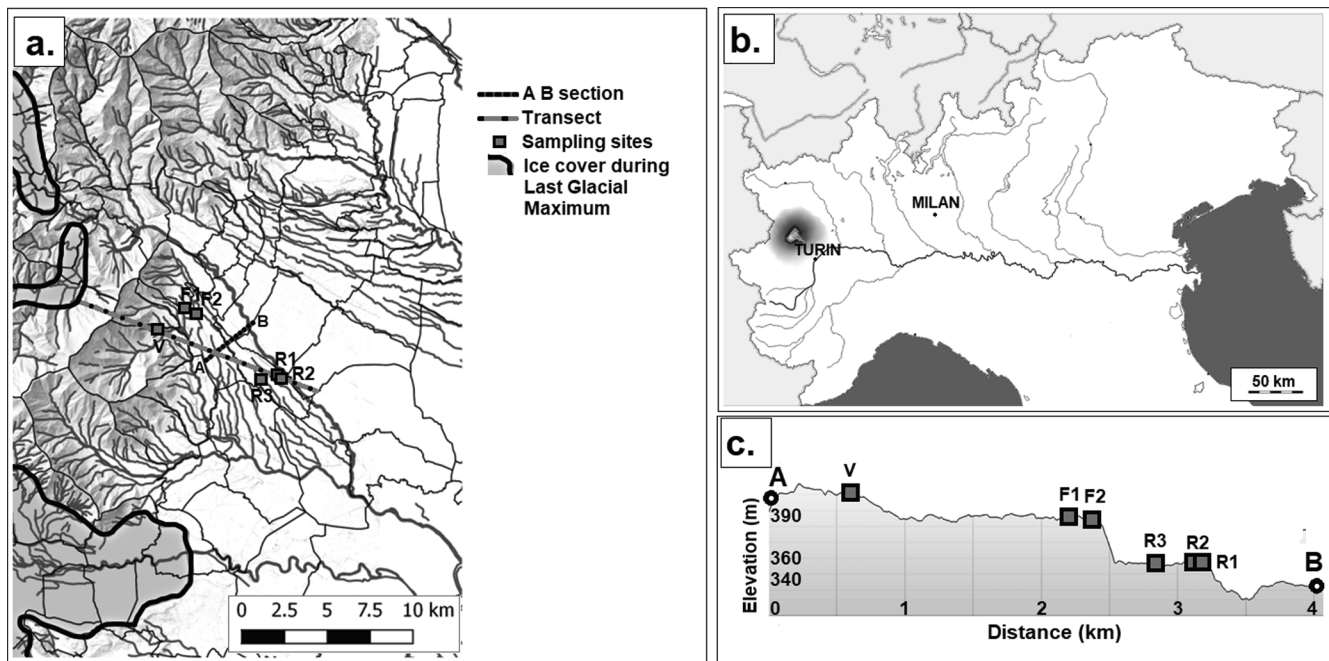
Fig. 1. (a) Study area with section of the terraced alluvial fan (AB), site locations, ice cover during Last Glacial Maximum (Ehlers et al., 2011) and NW-SE transect from the ice lobe that stood North to the study area across the Lanzo massif to the sampling points; (b) localization of the study area in Italy; (c) AB section of the alluvial fan with evident presence of terraced surfaces; lowest elevation found in correspondence of the Stura di Lanzo river bed (3.5 km from A).

Table1

Coordinates of the sampling sites in DMS format, with indication of the distance from ice lobe NW to the study area according to the NW-SE transect depicted in Fig. 1.

Site	Latitude (˚N)	Longitude (˚E)	Distance (km)
VA	45˚12′53.38″	7˚29′48.26″	5.01
F1	45˚13′35.54″	7˚30′56.31″	6.30
F2	45˚13′31.03″	7˚31′29.83″	7.06
R1	45˚11′21.83″	7˚34′27.51″	11.74
R2	45˚11′28.36″	7˚35′15.78″	12.61
R3	45˚11′25.43″	7˚35′15.89″	12.71

no loess older than Marine Isotopic Stage (MIS) 2 was found (ca. 29-14 ka BP). In Northern Italy, on the contrary, remnants of loess deposits ca. 72–38 ka old (MIS 4–3) have been recorded near Parma and Reggio-Emilia (Costantini et al., 2018). In Lombardy (Northern Italy) the well-known sequence of Monte Netto was attributed to the Upper Pleistocene, between MIS 2 and 4 (Costantini et al., 1996). Loess deposition in the Po plain has indeed been active at least since 60 ka BP, at the onset of glacial conditions in MIS 4 (Zerboni et al.,2015), and significant sedimentation rates have been recorded for that period (Costantini et al., 2018).

Soils that developed on loess are generally polycyclic and, often, a clear interbedding of loess sediments with developed soil horizons is visible (Muhs and Bettis, 2003). Typically, each pedostratigraphic level features a loess deposition belonging to a specific rhexistasy period in combination with evidence of multiple biostasy phases (Zerboni et al., 2015). The rhexistasy periods are characterized by the formation of thick loess blankets subdued to pronounced erosion (Rellini et al., 2009). These phases are not just followed, but generally interspersed, by vegetation cover and active pedogenesis.

The evaluation of soil development on loess is complicated, but a contribution may be given by the interpretation of loess particle morphology, providing clues on the origin of the loess material. The acquisition of detailed images of loess grains started back in the 70s (Smalley and Cabrera, 1970; Whalley and Krinsley, 1974), but shape characterization has been mainly addressed just qualitatively. To cite

some, the description of grain shapes was used to characterize loess beds (Assallay et al., 1996) and evidence of frost shattering on loess particles allowed the determination of transport distance (Cilek, 2001). Particle morphology, in terms of cavities, scratches, and cracks, was associated with weathering and glacial grinding in Northern France (Delage et al., 2005) while angular and rounded loess grains were related to fluvial and aeolian origin, respectively (Costantini et al., 2018). Notwithstanding the accepted relevance of particle shape in the assessment of loess deposits, quantitative analyses on grain shape parameters are generally lacking.

In addition to the multiplicity of units accountable in a single loess sequence, diagenesis tends to occur in deep-buried horizons and pedogenesis/pedodiagenesis is possible during loess deposition, given the slow cover rates induced by aeolian sedimentation (Schaetzl and Thompson, 2015). Investigating the homogeneity of the loess stratigraphy is fundamental to understand the genesis of soils in loess beds. The aeolian sediments may in fact have originated from different watersheds at different times, thus the present soil may not only show the record of different temporal and/or climatic pedogenic events (polycyclic feature) but also of different parent materials (polygenetic trait). Hence, the identification of lithological discontinuities is of primary relevance.

Therefore, the aim of this work was to characterize the soils developed on a loess formation in North-Western Italy, as a first step in the evaluation of the homogeneity of the sediments and the sources of the material. For this very purpose, a combination of field-derived morphological elements, laboratory analyses, and up-to-now underestimated quantitative image analysis techniques were applied.

2. Materials and methods

2.1. Study area, soil morphology and soil sampling

The study area (Fig. 1a) is represented by the South-Western side of the Stura di Lanzo (SL) alluvial fan, located in Piedmont (NW Italy, Fig. 1b). This terraced alluvial fan stretches over 300 km^2 at an elevation between 210 and 550 m.a.s.l. It is characterized by serpentinites,

Table 2
Morphological properties of the soil horizons, cycle of deposition, color.

Site (profile)	Horizon	Lower boundary (cm)	Cycle	Color (moist)	Mottles (colour, prominence)[a]	Coarse Fragments	Primary Structure[b]	Secondary structure	Boundary[c]	Clay coatings
VA	AE	23	V	10YR 4/2		–	M, W, SUB	M, W, G	CL	
	Bw1	38	V	10YR 4/3		---	M, W, SUB	M, W, PL	CW	
	Bw2	75	V	10YR 3/1	–	–	F, W, PL	–	AL	
	2Btx1	119	III	10YR 8/8	7.5YR 7/1, 5YR 4/4, vp	–	M, MO, PL	–	AW	+
	2Bv	123	III	7.5YR 2/2	10YR 8/8	–	M, MO, PL	–	AL	
	3Btx2	143	I	7.5YR 4/6	10YR 6/8, 5YR3/4,vp	–	C, STR, PL	–	AW	+
	3Bvm	148	I	5YR 2.5/1	5YR 2/1, vp-	–	C, STR, PL	–	AL	–
	4Btx3	190 +	S	5YR 4/6	10YR 6/8, vp	30%	C, STR, PL	–	U	+ +
F1	A	25	V	10YR 4/4	–	–	F, W, G	–	CW	
	Bw1	50/60	V	10YR 4/4	–	–	C, MO,SUB	–	CW	
	Bw2	60/70	V	10YR 4/6	–	–	M, W, SUB	–	AW	
	2Bc	70/80	I	7.5YR 4/6	–	–	C, W, SUB	M, W, A	CW	
	2Btc	90/100	I	5YR 4/4	5YR 4/3,wp	–	C, MO, BL	M, MO, A	CW	+
	2Bt1	110/115	I	5YR 4/6	–	1%	C, MO, BL	M, MO, A	GW	+ + +
	2Bt2	150/152	I	5YR 4/6	5YR 4/4,wp	–	C, MO, SUB	M, MO, A	AW	+ + +
	3Bt3	162	S	7.5YR 4/6		40%	C, STR, A	–	CL	+ + +
	3Btg	190/200	S	7.5YR 5/6	7.5YR 4/6	5%	C, STR, PL	–	CW	+ + +
	3Btx	230 +	S	5YR 4/6	10YR 5/6, 10YR 6/3, 5YR 4/6, vp	–	C, STR, PL	–	U	+ + +
F2	A	3	V	10YR 4/4	–	–	M, MO, G	–	AI	–
	A/B	50/65	V	10YR 5/8	–	–	M, MO, SUB	F, W, G	GW	–
	Bg	90	V	7.5YR 5/8	10YR 6/3, 2.5YR 4/6, wp	–	M, MO, BL	W, W, PL	AW	–
	2Bcx	100	IV	7.5YR 5/8	7.5YR 6/3, 2.5YR 4/3, mp	–	M, MO, SUB	–	CW	+
	2Btx1	115/120	IV	10YR 5/8	10YR 6/2, 2.5YR 4/6, mp	–	M, STR, SUB	F, MO, PL	CW	+
	2Btxc	165	IV	10YR 6/8	–	–	M, STR, SUB	–	AL	+
	3Btx	210/220	III	10YR 5/8	10YR 6/2 2.5YR 4/4,vp	–	C, STR, PL	–	AW	+
	3Bxc	215/225	III	10YR 5/8	2.5YR 2/2,vp	–	C, STR, PL	–	AL	–
	4Bx	255/260	II	10YR 6/8	10YR 3/6, 2.5YR 6/1, vp	–	C, STR, PL	SUB	AW	–
	5Bvm1	265	S	10YR 6/8	2.5YR 2/1, vp	–	C, STR, PL	–	AL	–
	5Bvm2	298 +	S	7.5YR 5/8	2.5YR 2/1, vp	10%	C, STR, PL	–	U	–
R1	A	20	V	10 YR 4/3	–	–	F, MO, G		AL	–
	Bw	60/85	V	10 YR 5/4	–	–	C, MO, SUB	S, W, A	CW	–
	2Bx1	100	IV	7.5YR 5/8	–	–	C, MO, P	–	AL	–
	2Bx2	140	IV	7.5YR 5/8	2.5YR 3/2, 10YR 6/3,wp	–	C, MO, P	M, W, PL	AW	–
	2Bx3	162	IV	10 YR 8/8	7.5YR 4/6, 5YR 7/8, wp	–	C, MO, P	M, W, PL	AL	–
	3Bv(x)t	190/196	III	10 YR 7/8	2.5YR 6/3, 10YR 5/8, vp	–	C, STR, PL	–	CI	+
	4Btx	220 +	II	10 YR 5/5	7.5YR 6/8, 10YR 6/3, vp	–	C, STR, PL	–	U	+ +
R2	A	22	V	10YR 4/3	–	–	M, W, G	–	AL	–
	Eg	93	V	7.5 YR 5/8	–	–	C, W, BL	–	AL	–
	2Bv	100/105	IV	7.5 YR 4/5	–	–	C, MO, BL	–	CW	–
	2Bx	123	IV	7.5 YR 6/8	7.5YR 4/6, wp	–	C, W, PL	–	CW	–
	2Btx	133/143	IV	7.5 YR 7/8	7.5YR 7/1, 10YR 5/6, wp	–	C,MO, PL	–	AW	+
	3Btx	143/150	III	7.5YR 4/6	10YR 6/4,vp	–	C, STR, PL	SUB	AW	+ +
	3Bv	160/165	III	10 YR 6/8	10YR 6/3, 10YR 5/8, vp	–	C, STR, BL	–	AI	–
	4Bvm	193	I	10YR 6/8	2.5YR 2/1, vp	–	C, STR, PL		CW	–
	4Btcg	220 +	I	10YR 5/6	10YR 6/3, 10YR 7/8, vp	–	C, STR, PL	F, STR, A	U	+ + +
R3	A	26	V	10 YR 4/4	–	–	M, W, G	–	AL	–
	Bw	57	V	10 YR 6/6	–	–	C, W, SUB	–	AL	–
	2Btx	72/80	IV	10 YR 5/8	2.5YR 6/8, 7.5YR 5/6, wp	–	C, MO, SUB	–	CW	–
	2E/Bx	102	IV	10 YR 5/8	2.5YR 7/8, 10YR 6/2, mp	–	C, MO, PL	A, BL	AL	–
	2Btxc	140	IV	2.5 YR 6/8	2.5YR 5/6, 2.5YR 6/2, mp	–	C, MO, PL	–	AL	+
	3Btx(v)	160/165	III	10 YR 4/4	7.5YR 5/1, mp	–	A, MO, BL	–	IW	+ +
	3Bx	180	III	10 YR 4/4	2.5YR 4/6, 2.5YR 3/4, mp	–	M, STR, A	–	AL	–
	4Bv(m)	200	II	7.5YR 6/4	2.5YR 8/4, 7.5YR 4/6, vp	–	C, STR, PL	–	CW	–
	4Bvm	215	II	7.5YR 3/4	10YR 7/8, 2.5YR 4/4, vp	–	C, STR, PL	–	AL	–
	5Btg(v)	230 +	S	10YR 5/8	2.5YR 6/8, 2.5YR 5/6, vp	–	C, PSTR, L	F, STR, A	U	+ + +

[a] Mottles:vp = very prominent, mp = moderately prominent; wp = weakly prominent;[b]Structure: F = fine, M = medium, C = coarse, W = weak, MO = moderate, STR = strong, A = angular, SUB = subangular, G = granular, P = prismatic, PL = platy, BL = blocky; [c]Lower Boundary: C = clear, G = gradual, A = abrupt, L = linear, W = wavy, I = irregular, U = unknown.

Table 3
Profile Development Index(PDI) values grouped according to loess depositional cycle. The parameters selected for PDI determination were: rubification, mottles, clay coatings development, cementation, structure, nodules, expression of fragipan and plinthic/petroplinthic horizons.

	Horizon	Rubification	Mottling	Clay films	Structure	Nodules	Fragipan	Plinthite	PDI horizon	PDI cycle	Cycle
VA	A/E	0.00	0.00	0.00	0.25	0.00	0.00	0.00	0.036	0.050	V
	Bw1	0.00	0.00	0.00	0.38	0.00	0.00	0.00	0.054		
	Bw2	0.00	0.00	0.00	0.38	0.00	0.00	0.00	0.054		
	2Btx1	0.50	0.25	0.25	0.75	0.00	0.75	0.00	0.357	0.369	III
	2Bv	0.50	0.50	0.00	0.75	0.50	0.75	0.50	0.500		
	3Btx2	0.33	1.00	0.50	1.00	0.25	1.00	0.00	0.583	0.618	I
	3Bvm	0.50	1.00	0.00	1.00	1.00	1.00	0.75	0.750		
	4Btx3	0.83	1.00	0.50	1.00	0.50	1.00	0.00	0.690	0.690	S
F1	A	0.00	0.00	0.00	0.25	0.00	0.00	0.00	0.036	0.055	V
	Bw1	0.00	0.00	0.00	0.50	0.00	0.00	0.00	0.071		
	Bw2	0.17	0.00	0.00	0.25	0.00	0.00	0.00	0.060		
	2Bc	0.33	0.00	0.00	0.50	0.50	0.00	0.00	0.190	0.263	I
	2Btc	0.33	0.00	0.25	0.50	0.50	0.00	0.00	0.226		
	2Bt1	0.50	0.00	0.75	0.50	0.25	0.00	0.00	0.286		
	2Bt2	0.50	0.25	0.75	0.50	0.00	0.00	0.00	0.286		
	3Bt3	0.67	0.00	1.00	0.50	0.25	0.00	0.00	0.345	0.489	S
	3Btg	0.67	0.00	0.75	1.00	0.00	0.00	0.00	0.345		
	3Btx	0.83	1.00	0.75	1.00	0.00	0.75	0.00	0.619		
F2	A	0.50	0.00	0.00	0.25	0.00	0.00	0.00	0.107	0.141	V
	A/B	0.50	0.00	0.00	0.25	0.00	0.00	0.00	0.107		
	Bg	0.67	0.50	0.00	0.25	0.00	0.00	0.00	0.202		
	2Bcx	0.50	0.50	0.00	0.50	0.50	0.50	0.25	0.393	0.376	IV
	2Btx1	0.67	0.50	0.25	0.50	0.25	0.50	0.00	0.381		
	2Btx2	0.50	0.50	0.25	0.50	0.25	0.50	0.00	0.357		
	2Btxc	0.50	0.50	0.25	0.50	0.75	0.50	0.50	0.500		
	3Btx	0.50	1.00	0.50	1.00	0.25	0.75	0.00	0.571	0.580	III
	3Bxc	0.50	1.00	0.00	1.00	0.75	0.75	0.75	0.679		
	4Bx	0.50	1.00	0.25	1.00	0.50	1.00	0.00	0.607	0.607	II
	5Bvm1	0.83	1.00	0.00	1.00	1.00	0.00	1.00	0.690	0.694	S
	5Bvm2	1.00	1.00	0.00	1.00	1.00	0.00	1.00	0.714		
	5Bvm3	1.00	1.00	0.00	1.00	1.00	0.00	0.75	0.679		
R1	A	0.00	0.00	0.00	0.25	0.00	0.00	0.00	0.036	0.036	V
	Bw	0.00	0.00	0.00	0.25	0.00	0.00	0.00	0.036		
	2Bx1	0.67	0.50	0.00	0.50	0.00	0.50	0.00	0.310	0.312	IV
	2Bx2	0.67	0.50	0.00	0.50	0.00	0.50	0.00	0.310		
	2Bx3	0.50	0.50	0.25	0.50	0.00	0.50	0.00	0.321		
	3Bv(x)t	0.50	0.75	0.50	1.00	0.00	1.00	0.00	0.536	0.536	III
	4Btx	0.17	1.00	1.00	1.00	0.00	1.00	0.25	0.631	0.631	II
R2	A	0.00	0.00	0.00	0.25	0.00	0.00	0.00	0.036	0.109	V
	Bw	0.17	0.00	0.00	0.25	0.00	0.00	0.00	0.060		
	Eg	0.67	0.25	0.00	0.25	0.00	0.00	0.00	0.167		
	2Bv	0.17	0.50	0.00	0.50	0.50	0.00	0.25	0.274	0.385	IV
	2Bx	0.67	0.50	0.00	0.50	0.25	0.50	0.00	0.345		
	2Btx	0.67	0.50	0.25	0.75	0.00	0.50	0.00	0.381		
	2Bv	0.67	0.50	0.00	0.75	0.75	0.00	0.50	0.452		
	3Btx	0.50	1.00	0.75	1.00	0.00	0.75	0.00	0.571	0.571	III
	3Bv	0.50	1.00	0.00	1.00	0.75	0.00	0.75	0.571		
	4Bvm	0.50	1.00	0.00	1.00	0.75	0.00	0.75	0.571	0.605	I
	4Btcg	0.17	1.00	1.00	1.00	1.00	0.00	0.25	0.631		
R3	A	0.00	0.00	0.00	0.25	0.00	0.00	0.00	0.036	0.049	V
	Bw	0.17	0.00	0.00	0.25	0.00	0.00	0.00	0.060		
	2Btx	0.50	0.25	0.25	0.50	0.00	0.25	0.00	0.250	0.339	IV
	2E/Bx	0.50	0.50	0.00	0.50	0.50	0.25	0.00	0.321		
	2Btxc	0.50	0.50	0.25	0.75	0.25	0.50	0.00	0.393		
	3Btx(v)	0.00	0.50	0.50	0.50	0.25	0.50	0.25	0.357	0.326	III
	3Bx	0.00	0.50	0.00	0.75	0.00	0.75	0.00	0.286		
	4Bv(m)	0.17	1.00	0.00	1.00	0.75	0.25	0.50	0.524	0.554	II
	4Bvm	0.17	1.00	0.00	1.00	1.00	0.00	1.00	0.595		
	5Btg(v)	0.83	1.00	1.00	1.00	0.25	0.00	0.50	0.655	0.655	S

lherzolites, prasinites, and amphibolites as dominant lithotypes (Servizio Geologico d'Italia, 2009).

Loess lies on the top of fluvial and fluvioglacial sediments, a mixture of deposits carried by the SL and the nearby Ceronda rivers. The dating of these sediments places their origin from 730 ka to 40 ka BP (Forno et al., 2007). The SL river watershed is characterized by ca. 60% ophiolitic outcrops (serpentinites and peridotites of the Piedmont ophiolite system) and 40% sialic gneiss belonging to the Sesia-Lanzo zone. The basin of the Ceronda river is completely carved into the Lanzo Ultrabasic Complex (Servizio Geologico d'Italia, 2009). Gravel and cobblestones of variable dimensions and weathering degree characterize these deposits (Forno et al., 2007). The river terraces (Fig. 1c) are covered by a sheet of aeolian loess, up to 3 m thick at some sites. There is no agreement in the literature on the dating of this loess. Some authors stated that the deposition happened between 100 and 40 ka BP (Forno et al., 2007), while other paleoclimatic investigations (e.g.
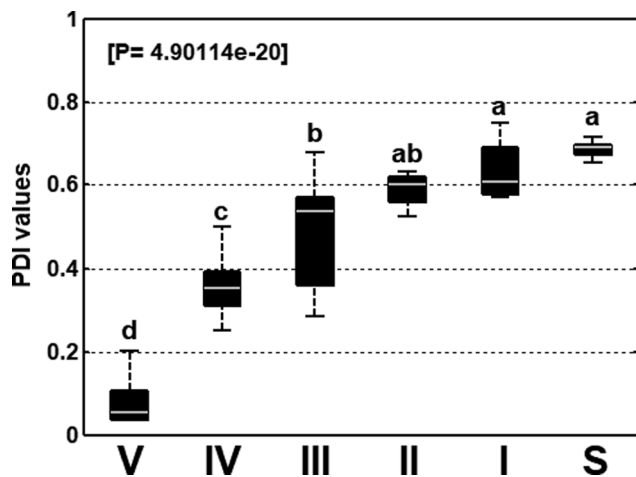
Fig. 2. PDI values of all horizons but F1 as grouped by cycle of belonging; substrate also considered (S).

Table 4
Particle size distribution determined by pipette method.

Site	Horizon	Cycle	Coarse Sand (%)	Fine Sand (%)	Coarse Silt (%)	Fine Silt (%)	Clay (%)
VA	Bw1	V	3	27	18	33	19
	Bw2	V	5	19	20	35	21
F1	Bw1	V	3	25	20	35	17
	Bw2	V	2	22	21	33	22
	2Bc	I	5	24	20	30	21
	2Btc	I	5	23	20	27	25
	2Bt1	I	6	25	14	27	28
	2Bt2	I	6	22	13	20	39
F2	A/B	V	9	19	17	31	24
	Bg	V	3	24	11	28	34
	2Btx1	IV	3	16	23	25	33
	3Btx	III	1	23	16	27	33
	4Bx	II	8	23	16	27	26
R1	Bw	V	2	27	30	25	16
	2Bx1	IV	4	28	25	25	18
	2Bx2	IV	4	28	25	26	17
	2Bx3	IV	5	28	20	26	21
	3Bv(x)t	III	6	27	22	23	22
	4Btx	II	4	23	19	24	30
R2	Eg	V	11	23	26	26	14
	2Bv	IV	10	28	18	24	20
	2Bx	IV	3	25	19	23	30
	2Btx	IV	2	19	17	22	40
	3Btx	III	2	26	23	22	27
	3Bv	III	6	22	17	21	34
R3	Bw	V	2	23	23	32	20
	2Btx	IV	3	28	21	27	21
	2E/Bx	IV	4	24	22	28	22
	2Btxc	IV	2	25	22	29	22
	3Btx(v)	III	4	27	17	24	28
	3Bx	III	4	19	21	22	34

Billard and Orombelli, 1986) assess that at a nearby site the lowermost of four loess layers could be ascribed to Gl 5 (1.8–1.0 Ma).

The whole area was not covered by glaciers during the Last Glacial Maximum (LGM), nor during more ancient glacial expansions, as the closest lobe of the ice (Fig. 1a) stopped right behind the Lanzo Massif (Ehlers et al., 2011).

This area is now mostly covered by crops. The native hardwood forests with predominance of oak (*Quercus robur* L.) and European hornbeam (*Carpinus betulus* L.) are preserved only in small and marginal portions of the area.

The soils of the upper terraces are Typic Fragiudalfs (IPLA, 2009),

characterized by the presence of the fragipan at 60–70 cm of depth. Soil sampling was carried out at 6 different sites: Varisella (VA), Fiano (F1, F2), and Robassomero (R1, R2, R3).

The sites were selected at increasing distance (Table 1) from the margin of the ice lobe which stood behind the Lanzo Massif during LGM along a NW-SE transect (Fig. 1a). At all sites, a soil profile was opened and described throughout according to the FAO guidelines (FAO, 2006). The transition between fluvioglacial alluvium and loess deposits, when reached in the excavated pit, was well visible in the field. Each soil profile displayed increasing development with depth and many pedogenic discontinuities could be recognized. A modified version of the Profile Development Index (PDI), following the approach suggested by Harden (1982) and Harden and Taylor (1983), was applied to evaluate existing differences between soil horizons in a semi-quantitative way. Given the high adaptability of PDI calculation according to soil types (Schaetzl and Thompson, 2015), 7 specific parameters were selected for the studied soils: rubification, clay coatings development, structural aggregation shape and aggregate strength, mottles, nodules, expression of fragipan and presence of plinthic/petroplinthic horizons. This procedure was performed based on the morphologic/diagnostic properties described in the field. The horizons were grouped according to the unit, or cycle, of belonging. The PDI values of horizons that belonged to the same cycle were summed, and the result was then normalized by the thickness of the layer, in order to take truncation into consideration. For those soil horizons that developed on loess, the freshest loess layer was considered as the starting point in the PDI determination. It was widespread at shallow depths in the study area, sometimes found in the lowest part of Bw horizons. This material was characterized by a 10YR 5/4 color and a weak blocky subangular structure, hinting at a minimal but still existing pedogenic development. For the deep horizons that did not develop on loess deposits, but rather formed from the alluvial sediments, the fresh alluvium from nearby rivers was considered as starting point. This material was structureless and olive-colored (5Y 5/4).

Samples were taken from the whole thickness of genetic loess-derived horizons, air-dried, and sieved at 2 mm. A total of 31 B, AB, or E soil horizons was considered. In particular, partly or completely cemented B horizons (namely Bv and Bvm) were not sampled, nor were those developed in the fluvioglacial alluvium.

2.2. Soil analyses

The relative abundance of coarse sand (2000–200 μm), fine sand (200–50 μm), coarse silt (50–20 μm), fine silt (20–2 μm), and clay (< 2 μm) was determined by the pipette method after dispersion of the samples with Na-hexametaphosphate (Gee and Bauder, 1986).

On 13 selected horizons, the particle-size distribution was also measured by laser diffraction using a Malvern Mastersizer 2000 (Malvern, UK), after sample dispersion with Na-hexametaphosphate.

Advantages and issues related with laser diffraction method in particle-size analyses can be found in literature (e.g. Fisher et al., 2017; Bittelli et al., 2019). Laser PSD data were acquired as 101 size classes at a fixed step of 0.166 φ, ranging from 15.61 φ (0.02 μm) to −1.00 φ (2000 μm). They were characterized both in terms of cumulative grain size curve and probability density function, this latter providing information on modal grain size values. Each peak was thus described in terms of position, with x values expressed both in φ and μm, and intensity, expressed by y values in %, σ, and Width at Half Maximum (WHM). Such parameters were determined using the Curve Fitting Tool of MATLAB R2012b. An approximation of the area under each peak was obtained by multiplying WHM by y values.

2.3. Image analyses

On 12 selected horizons, silt and fine sand were separated from the other size fractions with a combination of wet sieving, to remove coarse
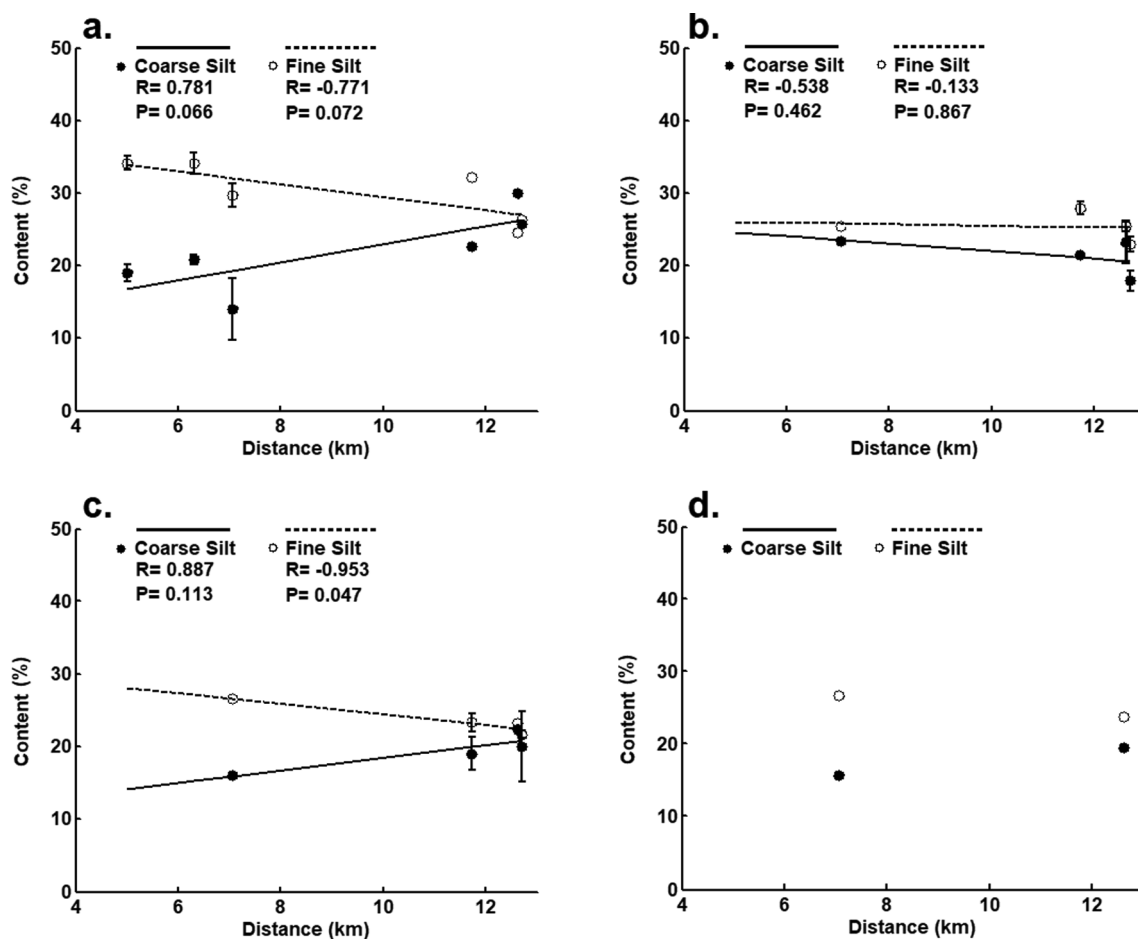
Fig. 3. Coarse and fine silt content trends along the NW-SE transect in each loess cycle deposition (average value and standard deviation). Figure: (a) cycle V, (b) cycle IV, (c) cycle III, (d) cycle II.

sand, and sedimentation, to remove clay. The selected material was analyzed by optical microscopy (630×) and image processing was applied to characterize the particle shape and color of the grains. After the digital enhancement of particle boundaries, the *Analyze Particles* command available in the ImageJ.exe software (https://imagej.nih.gov/ij/download.html) was implemented. All grains larger than 10 μm across were selected for the morphological assessment. The 10 μm cut-off was chosen in agreement with the minimum size of loess particles reported in the literature (Velichko et al., 2006). A number of 100–200 particles were analyzed for each soil horizon, allowing statistical data treatment (Sochan et al., 2015; Zerboni et al., 2015; Costantini et al., 2018).

For each grain, the *Analyze Particles* command calculated Aspect Ratio (AR), Roundness and Circularity according to the following equations:

$$AR = \frac{M_A}{m_A} \tag{1}$$

$$Roundness = 4 \times \frac{A}{\pi \times M_A{}^2} \tag{2}$$

$$Circularity = 4 \times \pi \times \frac{A}{P^2} \tag{3}$$

where M_A and m_A are, respectively, the major and minor particle axes (μm), A is the area (μm^2) and P is the perimeter (μm).

AR considers the ratio of the axes of the ellipse inscribable in a particle. It therefore corresponds to 1 in case of a circle and tends towards higher values with increasing elongation of the shape. Roundness value encloses the relative rounding of corners together with the

elongation of the particle, so that elongated shapes have lower roundness than equant shapes with some sharp corners (Blott and Pye, 2008). Roundness values vary from 0 to 1, with higher values for particles tending towards the shape of a perfect circle. Circularity, as defined by Cox (1927), takes into consideration the ratio of the area of the grain to the area of a circle with the same perimeter. It also ranges from 0 to 1 and has been recently recommended as one of the most reliable parameters describing the shape of a particle (Sochan et al., 2015).

The color of the particles was also evaluated using the Mean Gray value parameter present in the *Analyze Particles* command. This index gives, for each particle, the sum of the gray values of all the pixels in the selection divided by the number of the pixels. Thus, lower Mean Gray values correspond to darker particles.

2.4. Statistical analyses

MATLAB R2012b was implemented to perform all the statistical analyses. One-way ANOVA was used to investigate differences in the considered datasets, setting the threshold for statistical significance at the level of 0.05. Tukey-Kramer post-hoc test, default on MATLAB software, was applied.

3. Results

Several discontinuities were observed in the field based on changes in color, structure, and other pedogenic features (Table 2). Often, the boundary between two adjacent loess cycles was marked by Bc, Bv, or Bvm horizons. Five different depositional cycles were recognized in the field and named from I (oldest) to V (youngest) as visible in Table 2.
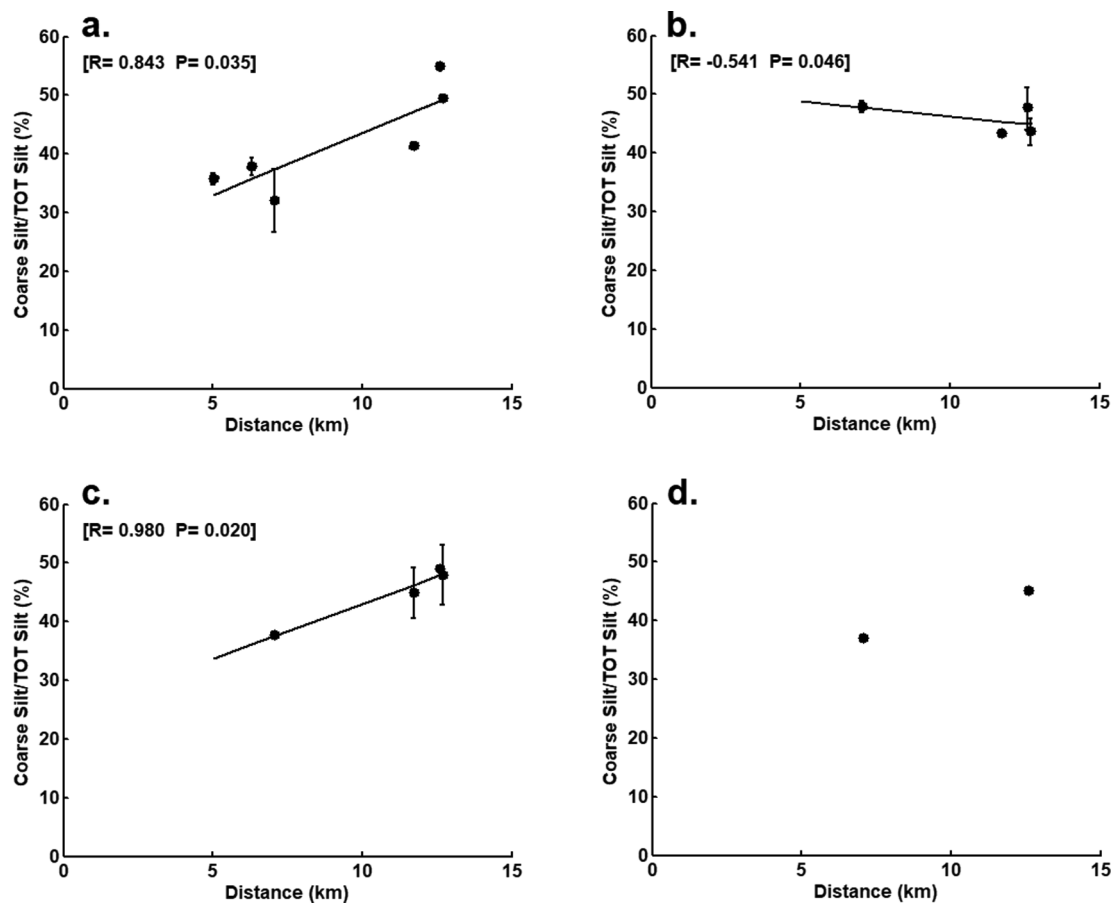
Fig. 4. Coarse silt to total silt content trends along the NW-SW transect in each loess cycle deposition (average value and standard deviation). Figure: (a) cycle V, (b) cycle IV, (c) cycle III, (d) cycle II.

The highly weathered alluvial or fluvioglacial substrate was called S-cycle. The oldest unit (I) was not found at all sites and its ancient origin was clearly highlighted by a great degree of reddening.

The results of PDI calculation are visible in Table 3, where horizon-specific parameters as well as cycle-referred normalized PDI values are displayed. An increase in pedogenic development degree with depth could be noticed in all the profiles, despite the differences in PDI values of top horizons. In particular, plinthic horizons close to the discontinuities were more developed and cemented with depth. Also, redder colors, more distinct mottles, and thicker clay coatings characterized the deeper horizons. The oldest loess deposition in F1, lacking in plinthic layers and with a paucity of hydromorphic features in general, displayed low PDI values. Excluding this profile, the PDI horizon values showed significant differences from one deposition to the other (Fig. 2).

Silt was the most abundant fraction in PSD (Table 4). The uppermost horizons belonging to cycle V displayed the greatest fine silt content, of around 30%. Coarse silt contents did not reveal any depth-related trend and ranged from 13 to 30%. The soils were characterized by little coarse sand content ($\leq$11%), while the amounts of fine sand ranged from 15 to 28%. Clay contents tended to increase towards the bottom of the profiles, from the most recent to the oldest depositional cycles, although the highest amounts of clay (40%) were found in a Bt horizon in the mid part of R2 profile. No significant differences were detected in size fractions contents from one deposition to the other but for fine silt, which was significantly higher in cycle V than in cycles III and IV (P < 0.001).

The fine and coarse silt contents showed a spatial trend alongside the considered transect, from NW to SE, when the deposition cycles were considered separately (Fig. 3). In cycles V (Fig. 3a), III (3c), and II

(3d) the coarse silt contents increased with increasing distance from the icecap that stood behind the Lanzo Massif, i.e. from VA to R1 (transect Fig. 1a). In those same cycles, fine silt contents displayed an opposite trend, i.e. decreasing with increasing distance. Cycle IV showed a different behavior as visible in Fig. 3b. Cycle I was not considered due to the limited number of samples available (n = 4, site F1). Not all the observed trends were statistically significant. Thus, to remove the contributions of all other size fractions, the relative abundance of coarse silt within the silt fraction (i.e. coarse silt/total silt) was calculated. The index was positively correlated to the distance from the icecap in cycles V and III (Fig. 4a and c, P = 0.035 and P = 0.020 respectively), but negatively correlated in cycle IV (Fig. 4b, P = 0.046). Despite only two samples from cycle II were available, a trend similar to those of cycles V and III was visible (Fig. 4d).

All laser-derived PSD functions showed the typical S-shaped loess curves, with notable differences upon increasing deposition age (Fig. 5a), and minor variations within the same cycle, among sites (Fig. 5b). The probability density PSD curves evidenced median size values of 6.5 φ (11.0 μm, Fig. 5c) in the youngest deposition and of 8 φ (3.9 μm) in the oldest one (Fig. 5d).

The probability density PSD curves of all the horizons showed a bimodal or tri-modal distribution (Table 5). The dominant mode corresponded to the fine silt class (M_{FSi}), around 8–14 μm. Another very important modal peak, always present, was visible in the clay class (M_c) or slightly above its upper limit, from < 1 μm (in most cases) up to 4 μm. It is worthwhile to note that M_c diameter values were slightly higher in the horizons developed on the oldest loess deposition. Except for the horizons with higher M_c diameters, all the others also showed a third modal peak in the fine sand class (M_{FSa}, 150–300 μm).

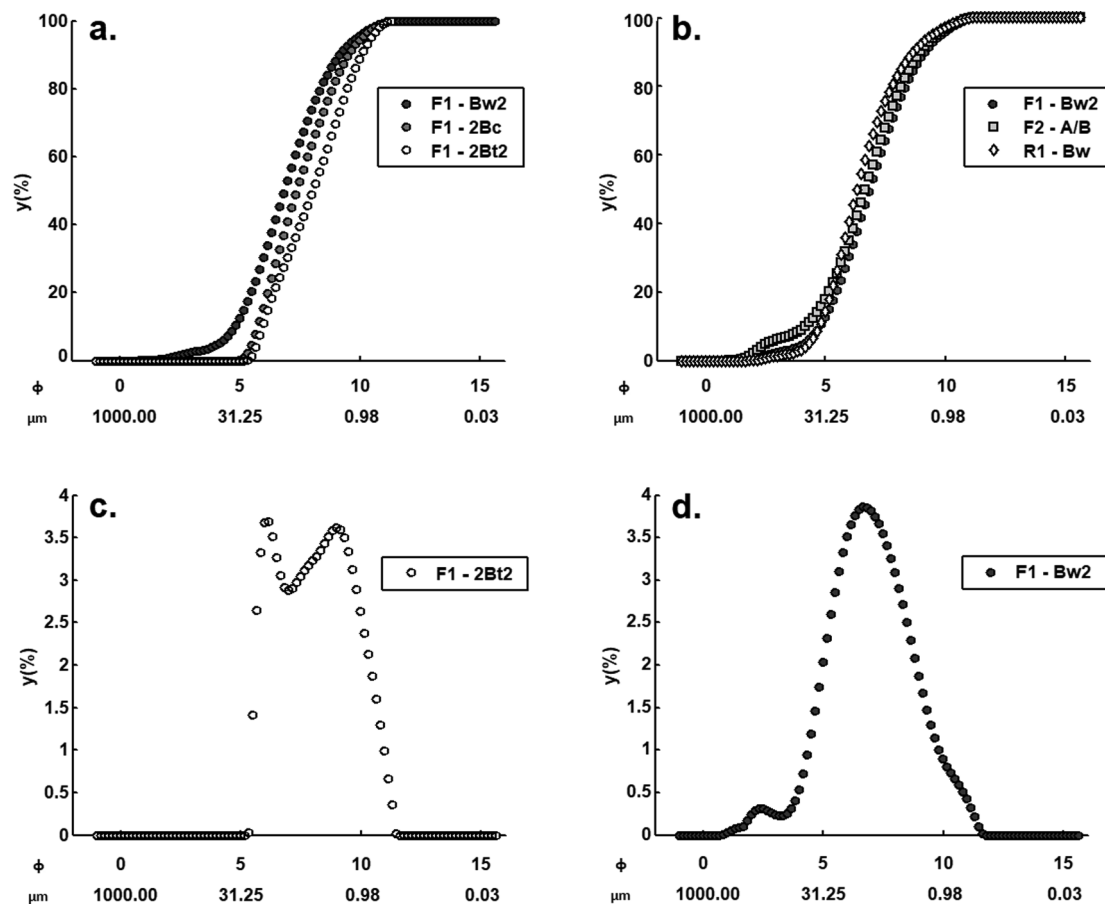Despite the noticeable trends, the diameter of the modal classes did

Fig. 5. PSD functions (a) cumulative curve of horizons belonging to different loess depositions within the same profile (cycles V, I, I); (b) cumulative curve of horizons belonging to the same loess deposition (V) at different sites; (c) probability density curve of a horizon belonging to loess deposition I; (d) probability density curve of a horizon belonging to loess deposition V.

not display any statistically significant difference among depositional cycles. A significant decrease (P < 0.01) in the peak area of M_{FSi} was instead visible from young to old depositions (Fig. 6a). The horizons belonging to cycle I had lower WHM values, i.e. they presented sharper peaks, than the others (Fig. 6b). The area of the finest modal class (M_c) showed an opposite trend, increasing significantly (P < 0.05) from young to old depositional cycles (Fig. 6c) due to broader peaks (Fig. 6d). Finally, MFSa showed no significant differences in height, WHM, or Area, but the presence of this modal fraction was not detected in all the horizons.

The results of image analysis, based on an average of 156 particles (10–200 μm range) for each soil horizon, are displayed in Table 6. Considering the deposition of belonging (Table 7), particles of cycles IV and I resulted significantly bigger than the others (P < 0.001). Roundness was significantly lower in cycle V (P < 0.05) as well as circularity (P < 0.001). AR was maximum in cycle IV and minimum in cycle III (P < 0.05), with intermediate values in the remaining depositions. Mean gray value was greatly lower for the particles belonging to cycle IV (P < 0.001), pointing towards the darker color of this material.

4. Discussion

In the analyzed loess-derived horizons, the evaluation of soil particles in terms of size, shape and color allowed to tell the existing differences in depositional events and to trace the possible origin of the loess material.

The selected profiles presented several cycles of loess deposition and, in all the studied horizons, laser-derived PSD cumulative curves

featured the S-shape typical of loess-derived materials (Cremaschi, 1987). In the SL soils, the predominant peak was always found in correspondence of fine silt (8–14 μm), evidencing a somehow homogeneous nature of the material. It is worth noting that the peak area in fine silt was smaller for the horizons developed on the oldest loess depositions. This fact was linked to lower WHM values (Fig. 6a, b), suggesting that weathering did not act upon loess producing a wider distribution in fine silt. Given the presence of quartz in a typical loess mixture (Smalley et al., 2006) and considering that quartz is more resistant to weathering with respect to other silicates (Smalley and Cabrera, 1970; Costantini et al., 2018), the observed distribution can be explained by a selective nature of the weathering process. The intensity of the modal peak in the size class between 0.5 and 4 μm (M_c) increased in the horizons developed on the oldest loess deposition. In these deeper horizons, the M_c modal size was however slightly bigger (2–4 μm) than in younger depositions (< 1 μm across). The increase in intensity for the smallest size class is in agreement with the development of clay minerals during pedogenesis (Zech et al., 2013), but the increase in radius is somehow surprising. To answer this, it should be considered that a final product of weathering and leaching during soil development is kaolinite, reported as a common component in loess soils of the USA (Dixon, 1989) but also present in many highly weathered soils developed on ultramafic rocks (e.g. Hseu et al., 2007). Kaolinite was often present in the bottom B horizons of other soils in the same study area (Raimondo et al., 2019) and its particles are slightly bigger than those of 2:1 highly charged layer silicates (e.g. Allen and Hajek, 1989).

One thing that really stood out in the analysis of the SL soils is the great abundance of fine silt, even in comparison to other loess-derived soils in Italy (Terhorst and Ottner, 2003; Costantini et al., 2018).

Table 5

Modal size classes obtained by peak fitting of laser diffraction PSD. Modes (peaks) in terms of position (x,y) , σ and Width at Half Maximum (WHM), Area and Percentage of the total Area.

Site	Horizon	Cycle	Peak	x (φ)	x (μm)	y (%)	σ (φ)	WHM (φ)	Area	Area %
F1	Bw2	V	M_{FSa}	2.53	172.78	0.31	0.68	1.60	0.50	2.97
			M_{FSi}	6.93	8.21	3.89	1.68	3.96	15.40	92.17
			M_c	10.46	0.71	0.65	0.53	1.25	0.81	4.86
	2Bc	I	M_{FSa}	–	–	–	–	–	–	–
			M_{FSi}	6.43	11.60	4.70	0.74	1.75	8.23	43.34
			M_c	8.19	3.43	3.34	1.37	3.22	10.75	56.66
	2Bt2	I	M_{FSa}	–	–	–	–	–	–	–
			M_{FSi}	6.25	13.12	3.94	0.54	1.28	5.04	34.27
			M_c	9.07	1.86	3.65	1.13	2.65	9.67	65.73
F2	A/B	V	M_{FSa}	2.29	204.62	0.87	0.51	1.20	1.04	6.72
			M_{FSi}	6.82	8.88	3.69	1.59	3.74	13.80	88.84
			M_c	10.51	0.69	0.56	0.52	1.23	0.69	4.43
	Bg	V	M_{FSa}	2.20	217.79	0.38	0.29	0.69	0.26	1.82
			M_{FSi}	6.36	12.22	3.99	1.38	3.26	13.01	90.17
			M_c	10.36	0.76	0.85	0.58	1.36	1.16	8.01
	2Btx1	IV	M_{FSa}	2.41	188.16	0.57	0.34	0.81	0.46	3.28
			M_{FSi}	6.41	11.78	3.87	1.40	3.30	12.77	90.85
			M_c	10.48	0.70	0.73	0.48	1.13	0.82	5.87
	3Btx	III	M_{FSa}	–	–	–	–	–	–	–
			M_{FSi}	6.37	12.07	4.14	1.39	3.26	13.50	92.93
			M_c	10.35	0.77	0.75	0.58	1.37	1.03	7.07
	4Bx	II	M_{FSa}	1.81	285.19	0.71	0.58	1.36	0.97	5.25
			M_{FSi}	6.43	11.59	3.83	1.14	2.69	10.30	56.03
			M_c	8.56	2.65	2.35	1.29	3.03	7.12	38.72
R1	Bw	V	M_{FSa}	2.57	168.87	0.26	0.39	0.92	0.24	1.50
			M_{FSi}	6.31	12.58	4.60	1.38	3.25	14.95	93.45
			M_c	10.21	0.84	0.55	0.62	1.47	0.81	5.05
	2Bx1	IV	M_{FSa}	1.71	305.87	0.27	0.56	1.32	0.36	2.62
			M_{FSi}	6.16	13.98	4.38	1.22	2.88	12.61	92.57
			M_c	10.46	0.71	0.58	0.48	1.13	0.66	4.81
	2Bx3	IV	M_{FSa}	2.00	249.83	0.54	0.73	1.72	0.93	6.84
			M_{FSi}	6.14	14.23	4.05	1.23	2.89	11.70	86.26
			M_c	10.32	0.78	0.72	0.55	1.30	0.94	6.90
	3Bv(x)t	III	M_{FSa}	2.70	154.00	0.43	0.36	0.85	0.37	1.77
			M_{FSi}	6.17	13.85	4.13	1.10	2.58	10.66	51.60
			M_c	7.93	4.11	2.61	1.56	3.69	9.63	46.63
	4Btx	II	M_{FSa}	–	–	–	–	–	–	–
			M_{FSi}	6.14	14.18	4.48	1.12	2.65	11.87	88.83
			M_c	10.06	0.94	1.14	0.56	1.31	1.49	11.17

Although weathering has certainly occurred and can be considered as one of the driving factors in the alteration of the original particle size distribution of wind-transported material, it cannot be addressed as the only responsible. The PSD cumulative curves reported by Ferraro et al. (2004) reached median values around 5 φ (31.3 μm). The same percentage, in our study, was obtained in correspondence of finer particles. A notable fact is that Zerboni et al. (2015) used cumulative grain size curves to distinguish fresh loess (median around 5.1 φ, 29.2 μm) from weathered loess (median around 7.5 φ, 5.5 μm), with intermediate values for intermediate degrees of weathering. In our samples, however, even young depositions, i.e. poorly weathered, displayed median values of 6.5 φ (11.0 μm), pointing towards a very peculiar nature of the loess in this area. And of course, when our oldest deposition was considered, the median value of 8 φ (3.9 μm) testified the gap with the above-mentioned similarly ancient and deeply weathered sediments. In general, the cumulative curves by Zerboni and colleagues exhibited higher intensity values in the range between 4 and 7 φ, regardless of deposition age, but the situation appeared reversed in the range between 7 and 9 φ. Therefore, the sole degree of weathering does not seem to be the main reason for the abundance of fine silt in the present study area. Under this light, comparing wind-blown sediments like alluvial-derived loess and last-glacial loess (Vandenberghe, 2013), the deposits of the SL resulted much more similar to the former than to the latter. PSD probability density curves of Chinese (Lu et al., 2012) and European (Marković et al., 2006) glacial loess sediments displayed a unimodal distribution, peaking in correspondence of ca. 5 φ (31.3 μm).

Alluvial loess (Vandenberghe et al., 2010), on the contrary, clearly evidenced a bimodal distribution, and the dominant peak in correspondence of 5 φ was coupled with a secondary peak close to 10 φ (1 μm). In this regard, it is worth mentioning that the Po Plain has been addressed not just in terms of a sedimentation site but also as an active source of loess (Costantini et al, 2018). Therefore, hypothesizing a dominant East-to-West paleo-wind direction, the loess now present in the SL area could have been carried from the plain towards the mountains. As widely accepted, aeolian transport produces size-dependent depositions (Sun et al., 2018) with coarser silts in the proximity of a loess source (Livingstone and Warren, 2019). Muhs and Bettis (2003) showed that with increasing distance (0–70 km) from a loess source a decrease in mean particle size (from 25 to 18 μm) could be observed. This happened in combination with an increase in fine silt (from 30 to 50%) and a decrease in coarse silt contents (60–40%). Despite the smaller scale, a similar distance trend could be appreciated also in the SL area. With growing distance from the glacial tongue that stood behind the Lanzo Massif during LGM (transect, Fig. 1a), an increase in coarse silt and a decrease in fine silt contents were observed in cycles V, III and II. This suggests that, in those glacial phases, the loess sediments were not transported alongside the transect with a NW to SE direction. On the contrary, they were rather wind-carried following the opposite direction. Other transects following different directions were drawn, but none of them gave good correlation and would univocally explain a size-dependent wind transport for all the cycles and the studied locations. A SE origin of the windblown sediments also justifies the
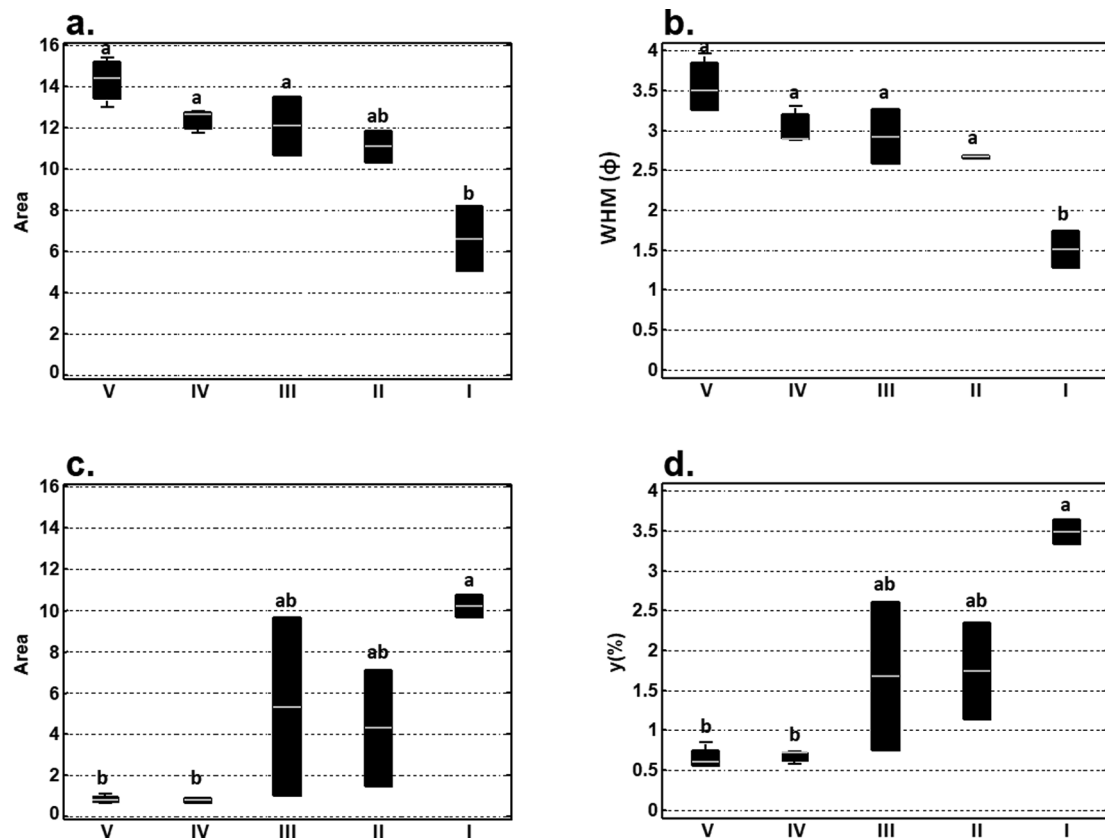
Fig. 6. Box plots for (a) Area of M_{FSi} according to deposition (p < 0.01); (b) WHM of M_{FSi} according to deposition (P < 0.01); (c) Area of M_C according to deposition (p < 0.01); (d) y of M_C according to deposition (P < 0.05).

Table 6
Morphological properties of soil particles as observed under optical microscope, size between 10 and 200 μm.

Site	Horizon	N° Part.	Longest side (μm)			AR			Circularity			Roundness			Mean Gray
			Mean	Median	ST dev	Mean	Median	ST dev	Mean	Median	ST dev	Mean	Median	ST dev	Median
VA	Bw2	197	17	14	8	1.84	1.58	0.87	0.63	0.65	0.11	0.62	0.63	0.18	131.96
F1	Bw2	102	19	15	9	1.70	1.52	0.50	0.68	0.69	0.09	0.63	0.66	0.15	98.02
	2Bc	101	22	18	13	1.71	1.52	0.57	0.70	0.72	0.10	0.64	0.66	0.17	138.16
F2	Bg	108	23	19	14	1.69	1.58	0.54	0.68	0.69	0.09	0.63	0.63	0.14	147.41
	2Btx1	164	21	17	12	1.76	1.49	1.28	0.69	0.71	0.11	0.65	0.67	0.16	106.70
	4Bx	161	19	15	10	1.65	1.56	0.47	0.71	0.72	0.10	0.64	0.64	0.15	111.40
R1	2Bx1	148	24	19	14	1.80	1.51	1.63	0.69	0.70	0.11	0.64	0.66	0.17	109.55
	3Bv(x)t	166	22	18	12	1.61	1.49	0.49	0.71	0.72	0.10	0.67	0.67	0.16	127.18
R2	3Btx	204	20	13	11	1.66	1.52	0.53	0.67	0.69	0.10	0.65	0.66	0.16	115.82
	3Bv	161	20	17	8	1.64	1.48	0.60	0.66	0.68	0.10	0.66	0.68	0.17	122.14
R3	Bw	151	20	17	9	1.69	1.54	0.59	0.64	0.66	0.12	0.64	0.65	0.17	124.75
	2Btx	216	21	17	12	1.74	1.51	0.95	0.68	0.70	0.13	0.65	0.66	0.17	113.56
	3Btx(v)	155	20	15	13	1.61	1.48	0.49	0.71	0.73	0.09	0.66	0.67	0.15	141.10

Table 7
Morphological properties of soil particles according to cycle of loess deposition.

| Parameters	V		IV		III		I		P value
	Mean	ST dev	Mean	ST dev	Mean	ST dev	Mean	ST dev	
Roundness	0.6294[b]	0.1631	0.6458[ab]	0.1683	0.6581[a]	0.1590	0.6379[ab]	0.1708	< 0.05
Circularity	0.6497[b]	0.1094	0.6837[a]	0.1186	0.6898[a]	0.0990	0.7009[a]	0.0987	< 0.001
AR	1.7441[ab]	0.6806	1.7615[a]	1.2717	1.6350[b]	0.5171	1.7100[ab]	0.5696	< 0.05
Mean Gray	127.2778[a]	26.2857	111.7905[b]	18.1940	125.5289[a]	25.1835	130.3689[a]	24.8517	< 0.001
Longest side	19.1620[b]	10.1826	21.6910[a]	12.7436	20.1930[ab]	11.0036	22.3454[a]	13.3230	< 0.001
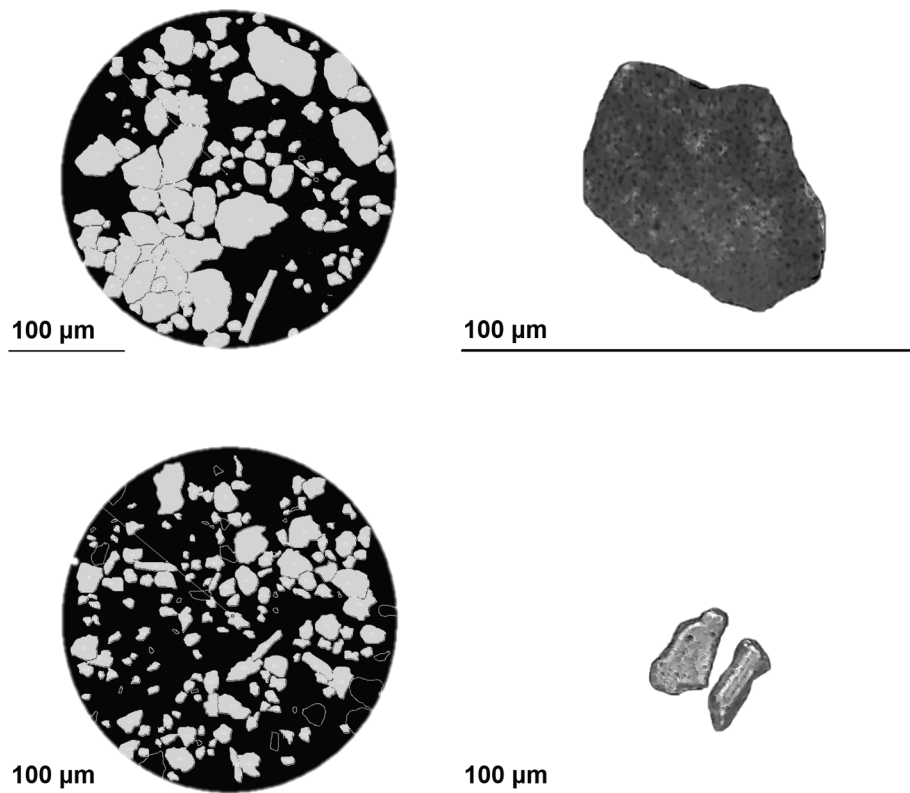
Fig. 7. Examples of glass slides and single particles belonging to cycle IV (top) and to cycle V (bottom).

hypothesized trend in quartz weathering we individuated from the analysis of the modal peaks in PSD-distribution. Quartz is in fact much more abundant in sialic and intermediate rocks than in the ultramafic lithologies of the SL massif. Regarding the loess deposited during cycle IV, an opposite distance trend was instead observed. It suggests that the origin of the material of that specific deposition has to be traced to some other source. The microscopic investigation revealed, on this matter, that the particles belonging to this cycle were not only significantly bigger and more elongated (Fig. 7; side and AR, Table 7) but also considerably darker in color (significantly lower Mean gray values, Table 7). Given the ultramafic nature of the Lanzo massif, a darker color would be expected from the particles arriving from that formation. Therefore, it can be assumed that during this exact cycle at least some of the wind-blown material came from the ice tongue and the massif adjacent to the SL area. The silt trends and the particles features (shape and color) seem thus to point in the same direction: the Po plain can be accounted as loess source in depositions V, III and II, while loess was originated and transported from behind the Lanzo Massif in deposition IV.

Finally, Roundness and Circularity did not display an increasing trend (greater values in smoother outlines) for older depositions. In agreement with other studies (Costantini et al., 2018), this points to the transport agent rather than the weathering process as the main shaper of grains in loess deposits.

5. Conclusions

The loess-derived soils of the SL area bear traces of an intense and long-standing pedogenesis, testified by remarkably reddish colors and the presence of sharply contrasting horizons within the same profile. Profile development was evaluated in a semi-quantitative way with the implementation of a modified version of PDI. This index included morphological features like the abundance of mottles/nodules and the expression of fragipan. The obtained results confirmed the cycle

distinction as it was evaluated in the field, evidencing that several depositional events of wind-blown material occurred in the area over time.

The studied loess deposits show a much greater abundance of fine silt with respect to other Italian loess deposits described in the literature. A possible answer to this uncommon trait would be considering the Po plain as the source of the material. This hypothesis was supported by the selection of the transported material according to size, observed in our study. Only the loess deposited during cycle IV, in fact, seems to have a different origin than the Po plain. Both the results of PSD analysis and image processing suggest that this material might instead have originated from the ice lobe which stood North to the Lanzo ultramafic massif. As a consequence of the multiplicity of sources, the study area is characterized by a mixture of lithologies with non-homogeneous susceptibility to weathering. Finally, it was possible to assess that loess particles were not primarily shaped by weathering, as the formerly deposited particles did not possess smoother edges.

The combination of the applied techniques allowed to support field-derived evidence of multiple depositional events, assessing in which terms the loess cycles were differing and trying to determine the most probable sources of the material. As the history of the polygenetic loess-derived SL soils is complex, both the variations in time and substrate, as soil forming factors, should be taken into account in further studies on the SL soils, but the same complexity may be present also in other pre-alpine environments.

Declaration of Competing Interest

The authors declare that they have no known competing financial interests or personal relationships that could have appeared to influence the work reported in this paper.

Acknowledgments

References

Allen, B.L., Hajek, B.F., 1989. Mineral occurrence in soil environments. In: Dixon, J.B., Weed, S.B. (Eds.), Minerals in Soil Environments. Soil Science Society of America, Madison, Wisconsin, pp. 199–278.

Assallay, A.M., Rogers, C.D.F., Smalley, I.J., 1996. Engineering properties of loess in Libya. J. Arid Environ. 32, 373–386.

Billard, A., Orombelli, G., 1986. Quaternary glaciations in the French and Italian pied-monts of the Alps. Quat. Sci. Rev. 5, 407–411.

Bittelli, M., Andrenelli, M.C., Simonetti, G., Pellegrini, S., Artioli, G., Piccoli, I., Morari, F., 2019. Shall we abandon sedimentation methods for particle size analysis in soils? Soil Tillage Res. 185, 36–46.

Blott, S.J., Pye, K., 2008. Particle shape: a review and new methods of characterization and classification. Sedimentology 55, 31–63.

Cilek, V., 2001. The loess deposits of the Bohemian Massif: Silt provenance, paleome-teorology and loessification processes. Quat. Int. 76–77, 123–128.

Costantini, E.A.C., Napoli, R., Bragato, G., 1996. Properties and geographic relevance of fragipan and other close-packed horizons in a non-glaciated Mediterranean region. Geogr. Fis. e Din. Quat. 19, 29–45.

Costantini, E.A.C., Carnicelli, S., Sauer, D., Priori, S., Andreetta, A., Kadereit, A., Lorenzetti, R., 2018. Loess in Italy: genesis, characteristics and occurrence. Catena 168, 14–33.

Cox, E.P., 1927. A method of assigning numerical and percentage values to the degree of roundness of sand grains. J. Paleontol. 1, 179–183.

Cremaschi, M., 1987. Paleosols and Vetusols in the Central Po Plain (Northern Italy): A study in Quaternary Geology and Soil Development. UNICOPLI, Milano, 306 pages.

Delage, P., Cui, Y.J., Antoine, P., 2005. Geotechnical problems related with loess deposits in Northern France. In: Proc. Int. Conf. on Problematic Soils, pp. 517–540.

Dixon, J.B., 1989. Kaolin and serpentine group minerals. In: Dixon and Weed (Eds.). Minerals in Soil Environments. Soil Sci. Soc. America, Madison, Wisconsin, USA, pp. 467–526.

Ehlers, J., Gibbard, P.L., Hughes, P.D., (Eds.), 2011. Quaternary Glaciations-extent and Chronology: A Closer Look. Elsevier, Amsterdam, NL. 1108 pages.

FAO, 2006. Guidelines for Soil Description, fourth ed. FAO, Rome.

Ferraro, F., Terhorst, B., Ottner, F., Cremaschi, M., 2004. Val Sorda: an upper Pleistocene loess-paleosol sequence in northeastern Italy. Rev. Mex. Ciencias Geológicas 21, 30–47.

Fisher, P., Aumann, C., Chia, K., O'Halloran, N., Chandra, S., 2017. Adequacy of laser diffraction for soil particle size analysis. PLOS ONE 12. https://doi.org/10.1371/journal.pone.0176510.

Forno, G.M., Gregorio, L., Vatteroni, R., 2007. La successione stratigrafica del settore destro del Conoide di Lanzo e il suo significato per l'utilizzo del territorio. Memorie Società Geologica Italiana. 87, 237–247.

Gee, G.W., Bauder, J.W., 1986. Particle-size Analysis. In: Klute, A. (Ed.), Methods of Soil Analysis, Part 1, second ed. Agronomy Monograph 9. Agronomy Society of America and Soil Science Society of America, Madison, Wisconsin, pp. 383–409.

Haase, D., Fink, J., Haase, G., Ruske, R., Pécsi, M., Richter, H., Altermann, M., Jäger, K.D., 2007. Loess in Europe-its spatial distribution based on a European Loess Map, scale 1:2,500,000. Quat. Sci. Rev. 26, 1301–1312.

Harden, J.W., 1982. A quantitative index of soil development from field descriptions: examples from a chronosequence in Central California. Geoderma 28, 1–28.

Harden, J.W., Taylor, E.M., 1983. A quantitative comparison of soil development in four climatic regimes. Quat. Res. 20, 342–359.

Hseu, Z.Y., Tsai, H., Hsi, H.C., Chen, Y.C., 2007. Weathering sequences of clay minerals in soils along a serpentinitic toposequence. Clays Clay Miner. 55 (4), 389–401.

IPLA, 2009. Carta dei suoli del Piemonte 1: 50000. Regione Piemonte. https://www.regione.piemonte.it/web/temi/agricoltura/agroambiente-meteo-suoli/carta-dei-suoli-150000.

Livingstone, I., Warren, A., (Eds.), 2019. Aeolian Geomorphology: A New Introduction. John Wiley & Sons, New York, USA, 336 pages.

Lu, H., Wang, X., Wang, X., Sun, X., Yi, S., Zhou, Y., Liu, Q.Y., Swineheart, J., Vandenberghe, J., 2012. Palaeoclimatic changes in northeastern Qinghai-Tibetan Plateau revealed by magnetostratigraphy and magnetic susceptibility analysis of thick loess deposits. Netherlands J. Geosci. – GeologieEnMijnbouw 91 (1–2), 189–198.

Marković, S.B., Oches, E., Sümegi, P., Jovanović, M., Gaudenyi, T., 2006. An introduction to the Middle and Upper Pleistocene loess-paleosol sequence at Ruma brickyard, Vojvodina. Serbia. Quat. Int. 149, 80–86.

Muhs, D.R., Bettis, E.A., 2003. Quaternary loess-paleosol sequences as examples of cli-mate-driven sedimentary extremes. Geol. Soc. Am. Spec. Pap. 370, 53–74.

Raimondo, E., Falsone, G., D'Amico, M., Stanchi, S., Celi, L., Bonifacio, E., 2019. Characteristics of fragipan B horizons developed on different parent material in North-Western Italy. Arch. Agron. Soil Sci. 65, 308–321.

Rellini, I., Trombino, L., Firpo, M., Rossi, P.M., 2009. Extending westward the loess basin between the Alps and the Mediterranean region: micromorphological and miner-alogical evidences from the northern slope of the ligurian Alps, Northern Italy. Geogr. Fis. e Din. Quat. 32, 103–116.

Schaetzl, R.J., Thompson, M.L., 2015. Soils. Soils: Genesis and Geomorphology, second ed. Cambridge University Press, pp. 795.

Servizio Geologico d'Italia, 2009. Carta geologica d'Italia 1:50000, foglio 155 e note il-lustrative. ISPRA e ARPA Piemonte, Direzione Regionale Servizi Tecnici e di Prevenzione.

Smalley, I.J., Cabrera, J.G., 1970. The shape and surface texture of loess particles. Geol. Soc. Am. Bull. 81, 1591–1596.

Smalley, I.J., Leach, J.A., 1978. The origin and distribution of the loess in the Danube basin and associated regions of East-Central Europe – a review. Sediment. Geol. 21, 1–26.

Smalley, I.J., Mavlyanova, N.G., Rakhmatullaev, K.L., Shermatov, M.S., Machalett, B., Dhand, K., Jefferson, I.F., 2006. The formation of loess deposits in the Tashkent re-gion and parts of Central Asia; and problems with irrigation, hydrocollapse and soil erosion. Quat. Int. 152, 59–69.

Smalley, I.J., Marković, S.B., 2014. Loessification and hydroconsolidation: there is a connection. Catena 117, 94–99.

Sochan, A., Zieliński, P., Bieganowski, A., 2015. Selection of shape parameters that dif-ferentiate sand grains, based on the automatic analysis of two-dimensional images. Sediment. Geol. 327, 14–20.

Sun, Z.X., Jiang, Y.Y., Wang, Q.B., Owens, P.R., 2018. A fractal evaluation of particle size distributions in an eolian loess-paleosol sequence and the linkage with pedogenesis. Catena 165, 80–91.

Terhorst, B., Ottner, F., 2003. Polycyclic luvisols in Northern Italy: palaeopedological and clay mineralogical characteristics. Quat. Int. 106–107, 215–231.

Vandenberghe, J., Gracheva, R., Sorokin, A., 2010. Postglacial floodplain development and Mesolithic-Neolithic occupation in the Russian forest zone. Proc. Geol. Assoc. 121, 229–237.

Vandenberghe, J., 2013. Grain size of fine-grained windblown sediment: a powerful proxy for process identification. Earth-Sci. Rev. 121, 18–30.

Velichko, A.A., Morozova, T.D., Nechaev, V.P., Rutter, N.W., Dlusskii, K.G., Little, E.C., Catto, N.R., Semenov, V.V., Evans, M.E., 2006. Loess/paleosol/cryogenic formation and structure near the northern limit of loess deposition, East European Plain, Russia. Quat. Int. 152, 14–30.

Whalley, W.B., Krinsley, D.H., 1974. A scanning electron microscope study of surface textures of quartz grains from glacial environments. Sedimentology 21, 87–105.

Zech, R., Zech, M., Marković, S., Hambach, U., Huang, Y., 2013. Humid glacials, arid interglacials? Critical thoughts on pedogenesis and paleoclimate based on multi-proxy analyses of the loess–paleosol sequence Crvenka, Northern Serbia. Palaeogeogr. Palaeoclimatol. Palaeoecol. 387, 165–175.

Zerboni, A., Trombino, L., Frigerio, C., Livio, F., Berlusconi, A., Michetti, A.M., Rodnight, H., Spötl, C., 2015. The loess-paleosol sequence at Monte Netto: a record of climate change in the Upper Pleistocene of the central Po Plain, northern Italy. J. Soils Sediments 15, 1329–1350.